Journal of The Electrochemical Society, **161** (3) A381-A392 (2014)
0013-4651/2014/161(3)/A381/12/$31.00 © The Electrochemical Society

Microelectrode Diagnostics of Lithium-Air Batteries

Iromie Gunasekara,[a,*] Sanjeev Mukerjee,[a,] Edward J. Plichta,[b] Mary A. Hendrickson,[b] and K. M. Abraham[a,**,z]**

[a]*Department of Chemistry and Chemical Biology, Northeastern University, Boston, Massachusetts 02115, USA*
[b]*Power Division, US Army RDECOM CERDEC CP&I, RDER-CCP, Aberdeen Proving Ground, Aberdeen, Maryland 21005, USA*

We demonstrate that a microelectrode can be used as a diagnostic tool to optimize the properties of electrolytes for non-aqueous Li-air batteries, and to elucidate the influence of ion-conducting salts on O_2 reduction reaction mechanisms. Oxygen reduction/evolution reactions on carbon microelectrode have been studied in dimethyl sulfoxide-based electrolytes containing Li^+ and tetrabutylammonium($(C_4H_9)_4N^+$) ions. Analysis of chronoamperometric current-time transients of the oxygen reduction reactions (ORR) in the series of tetrabutylammmonium (TBA) electrolytes, $TBAPF_6$, $TBAClO_4$, $TBACF_3SO_3$, $TBAN(CF_3SO_2)_2$ in DMSO revealed that the anion of the salt exerts little influence on oxygen transport. Whereas steady-state ORR currents(sigmoidal-shaped) were observed in TBA-based electrolytes, peak-shaped current-voltage profiles were seen in the electrolytes containing their Li salt counterparts. The latter response results from the combined effects of the electrostatic repulsion of the superoxide intermediate as it is reduced further to peroxide (O_2^{2-}) at low potentials, and the formation of passivation films at the electrode. Raman spectroscopic data confirmed the formation of Li_2O_2 and Li_2O on the microelectrode surface at different reduction potentials in Li salt solutions. Out of the four lithium electrolytes, namely $LiPF_6$, $LiClO_4$, $LiCF_3SO_3$, or $LiN(CF_3SO_2)_2$ in DMSO, the $LiCF_3SO_3$/DMSO solution revealed the most favorable ORR kinetics and the least passivation of the electrode by ORR products.
 [DOI: 10.1149/2.073403jes]

Manuscript submitted October 28, 2013; revised manuscript received December 9, 2013. Published January 7, 2014.

Li-air batteries, composed of Li metal anodes and oxygen cathodes in combination with non-aqueous electrolytes, have the potential to deliver practical rechargeable batteries with up to ten times more energy density than Li-ion batteries.[1,2] However, the reactivity of the oxygen reduction reaction (ORR) products, LiO_2 and Li_2O_2, toward the organic solvents used for electrolytes, and the irreversibility of the ORR processes remain as deterrents to these batteries from becoming practical systems.[3–6] Although, significant progress has been made in elucidating the redox chemistry of oxygen in non-aqueous Li-air batteries,[3,4,6,7] a full understanding of the factors affecting the oxygen electrode processes, particularly the ability to delineate mass transport contributions from electron transfer kinetics, is still lacking. In this regard, microelectrodes can provide information that cannot be obtained with the use of the traditional macroelectrodes employed in most ORR investigations.

Electrochemical data gathered using microelectrodes can be used to distinguish reactions controlled by mass transport from those dominated by electrode kinetics. In ideal cases, current-voltage data for an electrochemical process on a microelectrode exhibit limiting currents if there is no inhibition of mass transport. Deviation of the current-voltage response from this behavior is indication of possible mass transport limitations in the electrode reaction arising from a variety of sources. Poor solubility or high viscosity of the reaction products is a root cause. A prior oxygen electrochemistry investigation at a micro-cavity powder electrode has shown that the perfluorinated additives increases the oxygen solubility and the Li-O_2 cell performance.[8] A similar study by these authors showed that addition of acetonitrile to the electrolyte increases O_2 solubility by means of decreasing viscosity.[9] Another factor for deviation of the current-voltage data from limiting current response is the loss of effective electrode area by passivation films that hinder electrode activity thereby reducing the limiting current even at sufficiently high over potentials. Finally, if the reaction involves anionic reactants, at voltages sufficiently negative than the potential of zero charge of the electrode, the electrode can exert an electrostatic repulsion on negatively charged species.[10] In such cases, the electrode will produce a non-steady state, peak-shaped, response instead of the limiting current behavior.

Charging currents are close to zero on microelectrodes and, as a result, accurate electrode responses can be obtained even at high scan rates which is especially important to investigate fast electrode reactions followed by chemical dissociation of the products as observed in Li-air batteries.[11] Furthermore, microelectrodes are useful for studying very small volumes of electrolyte and since the reactions occur at homogeneous local physical environments, the current normalized on the electrode can give an accurate picture of the electrolyte/electrode interface behavior. Finally, microelectrode array systems can be used to experimentally characterize the site-dependent electrochemistry of a cathode catalyst which is relevant to ORR in non-aqueous Li-air batteries.

Investigations have been carried out on electrolytes in organic carbonate solvents for Li-O_2 batteries[12,13] in order to optimize solvent polarity so that the electrolyte does not flood the air cathode. However studies[5] have revealed that many organic carbonate solvents are unstable in the presence of the ORR intermediate, superoxide, O_2^-. Relatively stable solvents for use in Li-air batteries include ethers such as dimethoxy ethane (DME) and tetraethylene glycol dimethyl ether (TEGDME), organic sulfoxides and sulfones typified by diemthyl sulfoxide (DMSO), and ionic liquids exemplified by 1-ethyl-3-methylimidazolium bis(trifluoromethylsulfonyl)imide (EMITFSI) and 1-methyl-1-butyl-pyrrolidinium bis-(trifluoromethanesulfonyl)imide (PYRTFSI).[14] In this paper, we report on a detailed study of the use of microelectrodes for elucidating the influence of a series of ion-conducting salts on ORR in dimethyl sulfoxide-based electrolytes. Our results of the current-voltage response of the microelectrode reveal that the cation of the ion-conducting salt in the electrolyte plays a significant role on the properties of the ORR products. Detailed analysis of the microelectrode response has also shown that the triflate anion may have a positive influence on the stability and solubility of the ORR products in $LiCF_3SO_3$ solutions leading to the most favorable ORR kinetics. We demonstrate that the microelectrode can be used as a diagnostic tool to select and optimize the properties of electrolytes for use in non-aqueous Li-air batteries, and to elucidate the influence of different ion-conducting salts on oxygen redox reaction mechanisms.

Experimental

Materials.— All Lithium salts (lithium hexafluorophosphate, lithium perchlorate, lithium trifluoromethanesulfonate, lithium bis (trifuoromethanesulfonyl) imide and tetrabutylammonium salts (tetrabutylammonium hexafluorophosphate, tetrabutylammonium perchlorate, tetrabutylammonium trifluoromethanesulfonate, tetrabutylammonium bis (trifuoromethanesulfonyl) imide) and anhydrous grade solvents used in this study were purchased from Sigma-Aldrich and stored in M-Braun glove box maintained under 1 ppm humidity level.

*Electrochemical Society Active Member.
**Electrochemical Society Fellow.
zE-mail: kmabraham@comcast.net

Silver wires and 99.9% lithium foil were purchased from Alfa Aesar. The electrochemical half-cell employed a Pt mesh counter electrode, 11 μm diameter glassy carbon working electrode and a Ag/ Ag^+ reference electrode. This reference electrode was constructed as reported by Wain et al.[15] The Ag/ Ag^+ reference electrode potential with respect to the Li/ Li^+ reference electrode was determined by measuring the potential difference between a clean Li foil and the Ag/Ag^+ reference electrode immersed in the same electrolyte. This value was found to be 3.62 V in all electrolytes. All the data gathered on the carbon microelectrode are normalized to its geometric area experimentally determined using ferrocene oxidation current in DMSO. Potential step chronoamperometric transients for ORR were recorded in tetrabutylammonium (TBA^+)-based electrolyte solutions at the 11 μm carbon microdisc electrode. Cyclic voltammetric responses were recorded in all Li^+- and TBA^+-based electrolytes at scan rates up to 1000 mV s^{-1}. Supplementary electrochemical experiments for supporting the microelectrode analysis were carried out on a glassy carbon disk electrode (diameter = 0.59 cm). In order to characterize the ORR products, they were electro-deposited on a removable tip glassy carbon disk electrode by holding the electrode at a high enough over-potential for 60 min in O_2 saturated Li^+/DMSO and TBA^+/DMSO electrolytes. The products were analyzed by Scanning Electron Microscopy (SEM) and Energy Dispersive X-ray Spectroscopy (EDAX). Raman spectra were obtained for carbon cloth electrodes potentiostated for 5 hr periods at 2.12 V and 2.32 V respectively in O_2 purged $LiPF_6$ /DMSO electrolyte. Conductivities of the electrolytes of interest were measured using a Thermo-Orion conductivity cell and a Thermo-Orion conductivity meter. Kinematic viscosities of the solutions were recorded at 20°C using Ubbelohde Viscometer (C-545). FT-IR spectra were recorded for all four electrolytes on a Bruker ATR Infra-Red spectrometer.

Results and Discussion

Validation of the experimental approach and determination of the microelectrode radius.— A typical current-voltage response to electroactive species on a microelectrode, shown in Figure 1A for the oxidation of ferrocene to ferrocenium ion, illustrates the unique behavior of the microelectrode versus the macroelectrode response under identical experimental conditions (Figure 1B). The latter appears as the well-known cyclic voltammogram. The current-voltage response in Figure 1A displays a limiting current due to fast transport of the ferrocene molecules onto and the efficient removal of the oxidized ferrocenium products (zero reduction current) from the microelectrode surface by diffusion. As a result there is no reduction of the oxidized product on the return cathodic sweep on the microelectrode.

For a microelectrode operating under mass transport limited conditions, the limiting current, i_l, is a function of electrode radius r and it is given by equation 1.

$$i_l = \frac{4nFADC}{\pi r} = 4nFDCr \qquad [1]$$

In the above equation, n is the number of electrons, F is the Faraday constant, A is the electrode area, and D and C represent diffusion coefficient and concentration of the electroactive specie, respectively. Corresponding limiting current on a rotating disk macroelectrode is given by the Levich equation (equation 2) and it depends on the electrode rotation speed, ω, and the kinematic viscosity, υ, of the electrolyte.

$$i_l' = 0.620 \times nFAD^{\frac{2}{3}}\omega^{\frac{1}{2}}\upsilon^{-\frac{1}{6}}C \qquad [2]$$

Requirement to obtain a particular limiting current density in both electrodes can be derived by equating equations 1 and 2.[16]

$$0.62nFD^{2/3}\upsilon^{-1/6}\omega^{1/2}C = 4nFDC\pi^{-1}r^{-1} \qquad [3]$$

Equation 4 is obtained from equation 3 after canceling identical functions on both sides.

$$\omega^{1/2}r = \frac{4D^{1/3}\upsilon^{1/6}}{0.62\pi} \qquad [4]$$

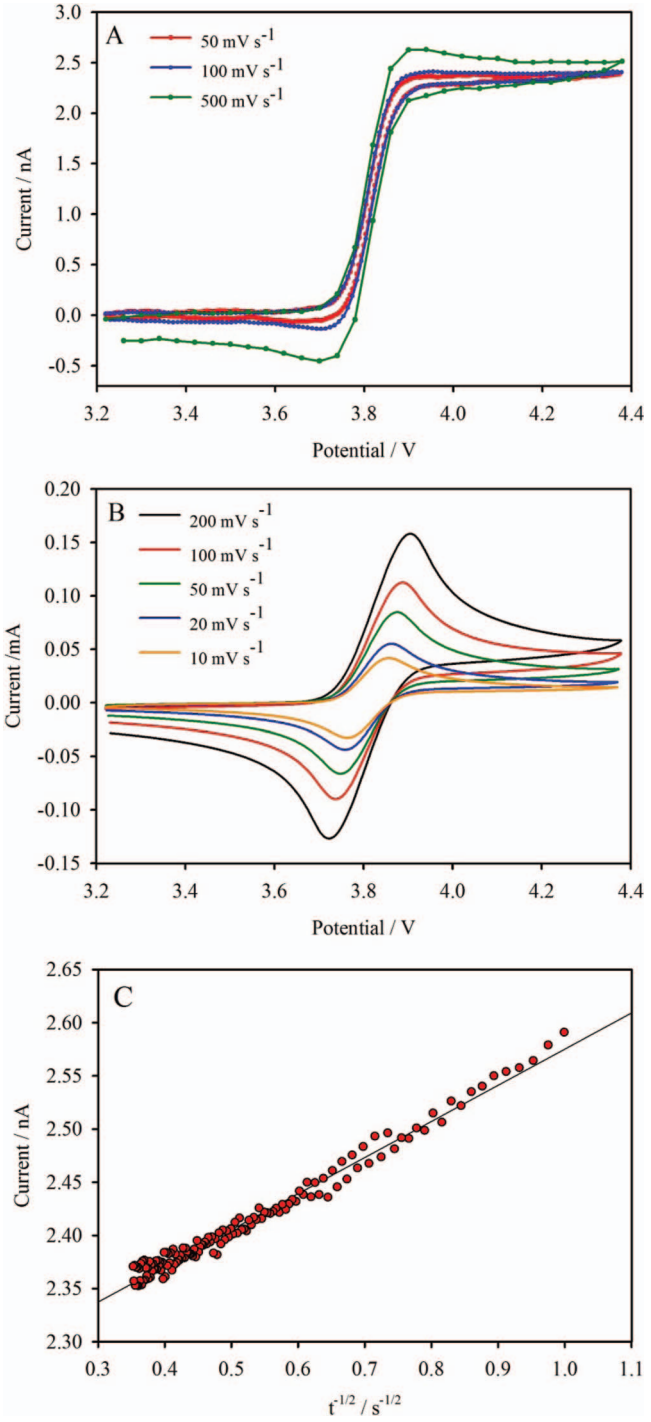

Figure 1. Ferrocene oxidation at the A): 11 μm microelectrode and B): glassy carbon disk macroelectrode. C): Current vs $t^{-1/2}$ plot for chronoamperometric transients obtained for the ferrocene solution on the microelectrode.

According to equation 4, a microelectrode radius of 5.5 μm corresponds to a rotation speed of ~25000 rpm (for $D_{O2,DMSO}$ ~ $2*10^{-5}$ cm^2s^{-1}, υ_{DMSO} ~1.9 cP) in a macrodisc electrode. Conventional rotors are designed for speeds of ~3000 rpm, hence much higher speeds are not achievable. Thus, microelectrodes yield current-voltage response under much higher mass transport rates than macroelectrodes. Voltammetric responses recorded under high rotation speeds on macroelectrodes often suffer from high iR drops which need to be carefully corrected by the use of solution resistances measured from high frequency AC impedance of the electrochemical

cell. One of the advantages of using microelectrodes is the negligible *iR* drop (high current density with minimal Ohmic polarization) due to the currents recorded at nano-Ampere range. Microelectrodes are particularly useful not only when high currents are involved but also when highly viscous solvents are to be analyzed in the absence of supporting electrolytes.

Oxidation of ferrocene to ferrocenium ions is a one-electron reaction and the diffusion coefficient (D) of ferrocene calculated by Janisch et al. for a 0.1–1.5 mM ferrocene solution in DMSO is $4.4*10^{-6}$ cm^2 s^{-1}.[17] Using this D and the limiting current in the 2.58 mM ferrocene solution (Figure 1A), the radius of the carbon microelectrode was calculated from equation 1 to be 5.54 μm. When the microelectrode potential is stepped from a potential where no reaction occurs to a potential where the reaction is diffusion limited, at small times after polarization, the diffusion limited current at a microelectrode is given by equation 5.[18,19]

$$I = \frac{nFAD^{\frac{1}{2}}C}{\pi^{\frac{1}{2}}t^{\frac{1}{2}}} + n\pi FDCr \qquad [5]$$

The diffusion coefficient and solubility of a reactive intermediate in the electrolyte can be calculated from the slope and the intercept of I vs. $t^{-1/2}$ curve.[19] Chronoamperometric transitions obtained by stepping the electrode potential from 3.62 V to 4.12 V were analyzed by the Cottrell plot (Figure 1C). Diffusion coefficient of ferrocene in DMSO was calculated to be $4.16*10^{-6}$ cm^2 s^{-1} and ferrocene solubility was found to be 2.95 mM for an electrode radius of 5.5μm. This calculated diffusion coefficient is in good agreement with the values determined above and those reported by other groups.[17] This validates the viability of our experimental approach for studying ORR on microelectrodes.

Kinetic equation for the reaction at the microelectrode under steady state conditions.— For a reaction in the form of $O + ne \leftrightharpoons R$, the steady state reversible current at the microelectrode is given by equation 6.

$$i^r = \frac{i_l}{\left\{1 + \frac{D_o}{D_R}\exp\left[\frac{nF\left(E-E^0\right)}{RT}\right]\right\}} \qquad [6]$$

This can be simplified to obtain equation 7, where E is the electrode potential, E^0 is the standard potential and i^r is the reversible current at the electrode.[20] D_O and D_R are diffusion coefficient of the oxidized and reduced species, respectively.

$$E = E^0 + \frac{RT}{nF}\ln\frac{D_R}{D_O} + \frac{RT}{nF}\ln\left[\frac{(i_l - i^r)}{i^r}\right] \qquad [7]$$

At $i^r = i_l/2$, the equation takes the form of 8, which allows us to calculate the diffusion coefficient of the (reduction) product, given that the D_O is known.

$$n\left(E^0 - E_{1/2}\right) = \frac{RT}{F}\ln\frac{D_O}{D_R} \qquad [8]$$

Diffusion coefficient of ferrocenium ion calculated in this way is 3.26×10^{-6} cm^2 s^{-1}. Equation 9 takes the difference between the experimental system and the reversible system in order to account for any irreversibility in the former. We apply this idea to analyze quasi reversible reactions[21] such as the lithium-oxygen system.

$$\left[\frac{4D_R}{\pi k_s r}\right]\exp\left[\frac{-nF\left(1-\alpha\right)\left(E-E^0\right)}{RT}\right] = \frac{(i_l - i)}{i} - \frac{(i_l - i^r)}{i^r} \qquad [9]$$

$$E - E^0 = \left[\frac{RT}{-nF\left(1-\alpha\right)}\right]\ln\left[\frac{4D_R}{\pi k_s r}\right] - \left[\frac{RT}{-nF\left(1-\alpha\right)}\right]\ln\left[\frac{(i_l - i)}{i} - \frac{(i_l - i^r)}{i^r}\right] \qquad [10]$$

In the above equations k_s is heterogeneous rate constant and α is the transfer coefficient of the reaction. Since the ORR electrochemistry in TBA salt/DMSO electrolyte is reversible, the experimental current in this system can be used as i^r. Similarly, the steady state limiting current in TBA salt/DMSO solution can be justifiably taken to be i_l in the Li-oxygen system. With these assumptions, the slope of the plot of $E - E^0$ vs. $\ln\left[(i_l - i)/i - (i_l - i^r)/i^r\right]$ allows us to calculate the transfer coefficient (α) for the initial reduction ($n = 1$) of O_2.

Deviation of microelectrode response from classical diffusion limited current.— The various factors that can produce a non-steady state current-voltage response on a microelectrode are discussed in this section.

1. *Passivation film formation*: As expected from equation 1, the current-voltage response will deviate from limiting current behavior if one of its parameters changes as the reaction proceeds. For example, insoluble reaction products deposited on the electrode surface will result in a change in the effective geometric radius with time. Furthermore, the diffusion coefficient of electroactive species (oxygen) through the film of insoluble products will be significantly lower. In such cases, the current response when measured as the potential is scanned, would take a peak type (akin to cyclic voltammogram on a macroelectrode) current-voltage profile.
2. *Migration of charged reactants away from the electrode surface due to electrostatic repulsion:* In some instances, the flux of the electroactive species onto the electrode surface will not be purely diffusion controlled. For example, transport of anionic reactants to a negatively charged electrode will be decreased due to electrostatic repulsion by the negatively charged electrode. Therefore, limiting current will be potential dependent. White et al.[10] described the migration-diffusion limited currents at a spherical microelectrode, by taking a new term called "interaction energy" into consideration.

$$A + e^- \rightarrow A^- \qquad [11]$$

$$A^- + e^- \rightarrow A^{2-} \qquad [12]$$

For example consider equation 11; the neutral reactant giving negatively charged products would give the expected sigmoidal shaped voltammogram. However, as in equation 12, if a singly negative reactant giving a doubly negative product, the shape of the voltammogram can deviate from a sigmoidal shape as the electrode potential is scanned toward negative potentials with respect to the potential of zero charge (E_{pzc}). In our study, the reaction of oxygen molecule going to superoxide represents the equation 11 and the superoxide ion reduction to peroxide ion is similar to the reaction in equation 12. In fact as presented below we consider this behavior as one of the reasons for the non-steady state microelectrode ORR response in Li salt solutions in DMSO.

Oxygen electrochemistry on carbon microelectrodes.— We have investigated the ORR current-voltage response at the microelectrode in a series of tetrabutylammonium and lithium salts solutions in DMSO. The salts studied included MPF_6, $MClO_4$, MCF_3SO_3, $MN(CF_3SO_2)_2$ where M = TBA or Li. Distinct differences in the current-voltage profile attributable to the TBA^+ and Li^+ salt solutions were observed, providing valuable insights into the strong influence of cation on the ORR electrochemistry and the mechanism of ORR in these electrolyte solutions.

ORR in Tetrabutylammonium (TBA) salt-based electrolytes.—Figures 2A and 2B show the voltammograms recorded on micro and macro electrodes, respectively, in oxygen-saturated solutions of 0.1 M $TBAPF_6$/DMSO. The limiting currents for oxygen reduction obtained for scan rates ranging from 50 to 1000 mV s^{-1} are seen in Figure 2A. The ORR is a one-electron reversible reaction in $TBAPF_6$/DMSO electrolyte as determined from detailed analysis of

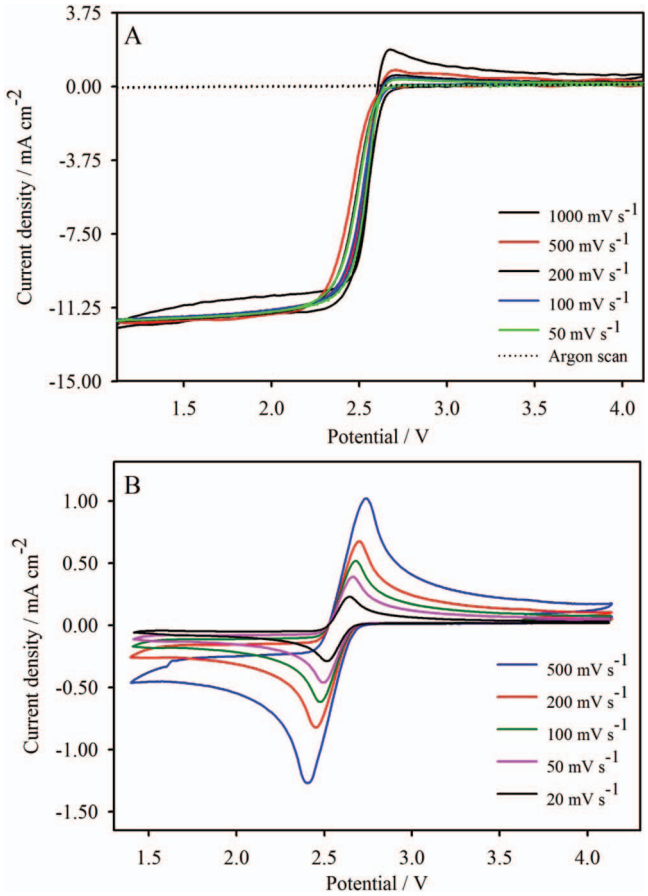

Figure 2. Current-voltage behavior observed in O_2 purged 0.1 M $TBAPF_6$/DMSO electrolyte at A): carbon microelectrode B): glassy carbon macroelectrode.

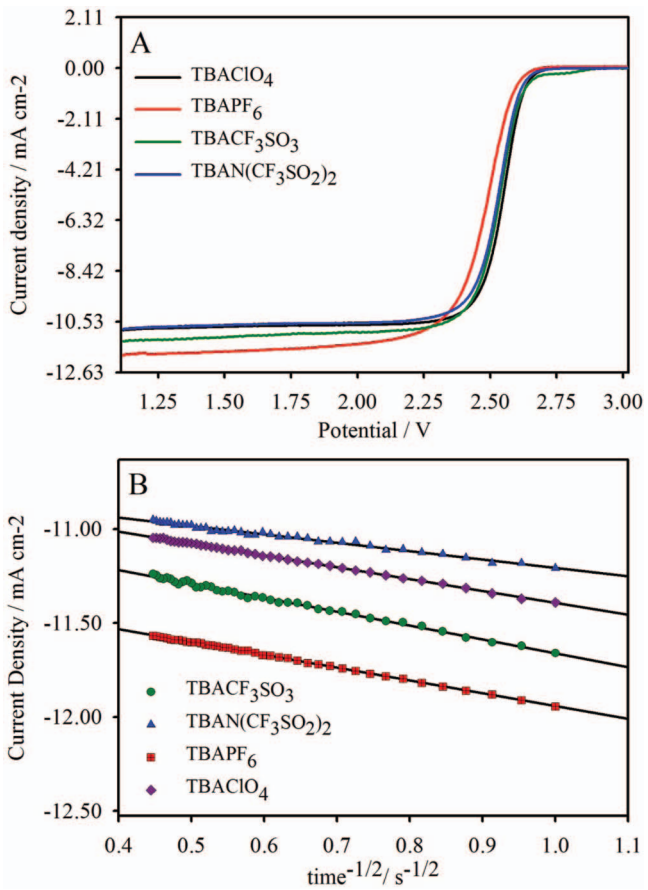

Figure 3. A): Oxygen reduction reaction on the microelectrode in 0.1 M TBA salts in DMSO at 50 mV s^{-1}. B): Cottrell plots calculated for the current time transients obtained by potential jump chronoamperometry experiments on the microelectrode in different TBA salt solutions in DMSO.

the data in Figure 2B using the Randles-Sevcik relationship as done previously.[4,7] As we have recently demonstrated through ^{13}C NMR chemical shift and spin-lattice relaxation time (T1) data in propylene carbonate solutions, TBA^+ is a soft acid due to its low charge density.[22] Therefore, TBA^+ interaction with the soft base O_2^-, the one-electron reduction product of O_2, is sufficiently strong to spare it from further reduction[4,7] at lower potentials. The nearly ideal limiting current behavior displayed in Figure 2A for a series of sweep rates indicates that the microelectrode surface is not modified by insoluble ORR products in TBA/DMSO electrolytes. The oxygen reduction product is apparently highly soluble in the electrolyte.

Similar ORR limiting currents were observed in 0.1 M $TBAPF_6$, $TBAClO_4$, $TBACF_3SO_3$, $TBAN(CF_3SO_2)_2$ in DMSO (Figure 3A). This suggests that the electrode process is primarily controlled by the TBA^+ cation with minimal influence by the anion on the ORR mechanism. Current-time transients obtained by stepping the electrode potential from 3.62 V to 1.62 V were analyzed using Cottrell equation as shown in Figure 3B. The oxygen diffusion coefficient and solubility in $TBAPF_6$/DMSO calculated from these data were found to be 2.2×10^{-5} cm^{-2} s^{-1} and 2.79×10^{-6} mol cm^{-3}, respectively.

The mass transport parameters presented in Table I show similar oxygen diffusivities in TBA^+ salt solutions with PF_6^-, ClO_4^- and $CF_3SO_3^-$ anions, whereas in the $N(CF_3SO_2)_2^-$-containing salt solution this value is slightly higher. In general, the data in Table I are in good agreement with those reported previously determined using macroelectrodes.[23,24] Xu et al. have also reported that oxygen solubility is not significantly affected by the lithium salt anion in carbonate based electrolytes.[13] The oxygen permeability represents the product of oxygen diffusion coefficient and its solubility and is a useful parameter for Li-O_2 cell modeling. Superoxide diffusion coefficients calculated using half wave potentials (equation 8) are also shown. The D_{O2}- values are significantly lower than D_{O2} calculated for the different electrolyte systems. Strong ion pairing between the superoxide ion and the bulky TBA^+ ions seems to decrease the diffusivity of O_2^- in these electrolytes. In an attempt to explain the observed trend in oxygen diffusion coefficient seen in Table I, we measured the physical properties of the electrolytes of interest and are depicted in Table II. The anion donor numbers previously calculated in dichloroethane solutions[25] are also presented in this table. Perchlorate-based electrolytes have the highest conductivities whereas the bis (trifluoromethanesulfonyl) imide solutions exhibit the lowest conductivities probably due to the low mobility of this large anion. However the conductivity differences are small.

ORR in Lithium ion-containing electrolytes.—Figure 4B displays the scan rate dependent current-voltage curves obtained on the microelectrode in oxygen saturated 0.1 M $LiPF_6$ in DMSO. The current reached its maximum at around 2.5 V (at 50 mV s^{-1}) and started to decrease at lower potentials. Most interestingly, the current-voltage curve has the appearance of a cyclic voltammogram. There was no sigmoidal shaped limiting current behavior as observed for O_2 in TBA salt-containing solutions. Considering that ORR limiting currents are observed in TBA^+/DMSO electrolytes, clearly this behavior is not arising from oxygen mass transport limitation in the electrolyte. On the contrary, it probably arises either from the passivation of the electrode by the deposition of insoluble lithium oxides on the electrode surface or due to limited reactant transport which is not purely diffusion controlled. Any insoluble products formed on the electrode would block enough O_2 from reaching the electrode surface to maintain a limiting current. In this context, it is useful to recall that previous

Table I. Oxygen mass transport parameters in TBAX electrolytes.

Salt	Oxygen Diffusion coefficient / $cm^2 \cdot s^{-1}$	Oxygen Solubility/mol. cm^{-3}	Oxygen Permeability/ mol. cm^{-1} s^{-1}	$E_{1/2}$/V	Superoxide Diffusion coefficient /cm^2 s^{-1}
$TBAPF_6$	2.2×10^{-5}	2.79×10^{-6}	6.14×10^{-11}	2.48	3.60×10^{-7}
$TBAClO_4$	2.3×10^{-5}	2.92×10^{-6}	6.72×10^{-11}	2.55	4.68×10^{-6}
$TBACF_3SO_3$	1.8×10^{-5}	3.89×10^{-6}	7.00×10^{-11}	2.53	1.65×10^{-6}
$TBAN(CF_3SO_2)_2$	4.7×10^{-5}	1.43×10^{-6}	6.72×10^{-11}	2.53	4.31×10^{-6}

Table II. Physical properties of the electrolytes at 20°C.

Electrolyte in DMSO	Viscosity / cSt	Conductivity / mS. cm^{-1}	Donor number of the anion[25]
0.1 M $LiPF_6$	2.13	2.10	2.50
0.1 M $TBAPF_6$	2.15	2.01	
0.1 M $LiCF_3SO_3$	2.09	2.06	16.90
0.1 M $TBACF_3SO_3$	2.15	1.87	
0.1 M $LiN(CF_3SO_2)_2$	2.32	2.04	5.40
0.1 M $TBAN(CF_3SO_2)_2$	2.11	1.65	
0.1 M $LiClO_4$	2.16	2.26	8.44
0.1 M $TBAClO_4$	2.19	2.10	

studies on macroelectrodes have shown that in presence of small cations like Li^+ and Na^+, ORR becomes less reversible[4,7] probably due to the precipitation of the corresponding peroxide and monoxide on the electrodes.

Figure 4A shows current-voltage behavior obtained on microelectrodes in O_2-purged $LiPF_6$/DMSO electrolyte for various cathodic limits. A small anodic peak was observed when the cathodic potential was limited half-way through the first reduction peak. The peak separation between the cathodic and anodic peaks in this case was much higher than 59 mV suggesting that the anodic peak is not arising from superoxide oxidation. The multiple anodic peaks and the large peak separation are similar to those observed by Cormac et al.[4] for ORR at a

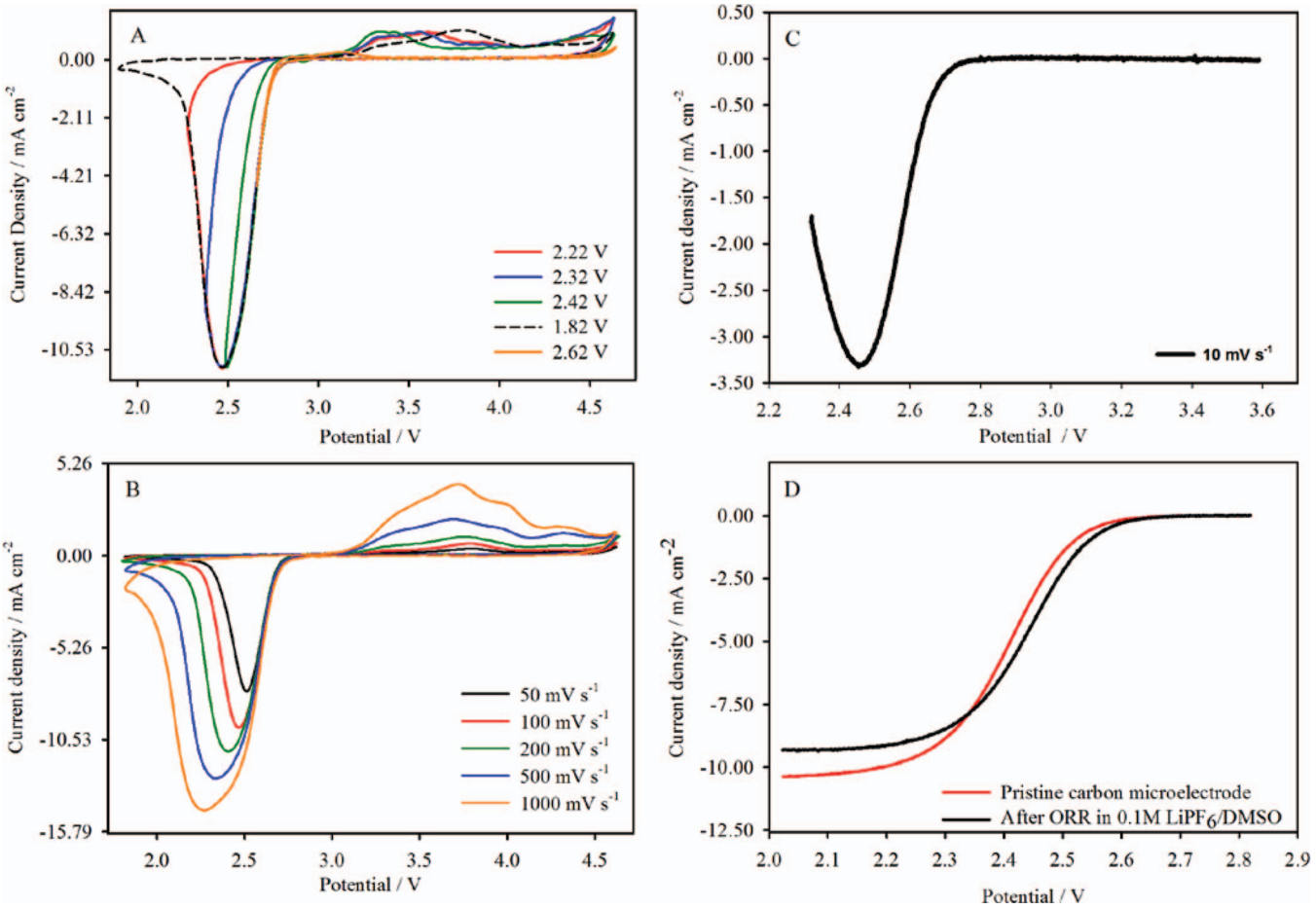

Figure 4. Current -voltage characteristics at the carbon microelectrode for O_2 purged 0.1 M $LiPF_6$/DMSO recorded: A) at various potential windows B), at scan rates ranging from 50–1000 mV s^{-1}, C) Oxygen reduction half-cycle in 0.1M $LiPF_6$/DMSO to passivate the electrode for the test in D, D) ORR currents obtained in 0.1M $TBAPF_6$/DMSO on the electrode after the oxygen reduction half-cycle in 0.1M $LiPF_6$/DMSO as shown in C.

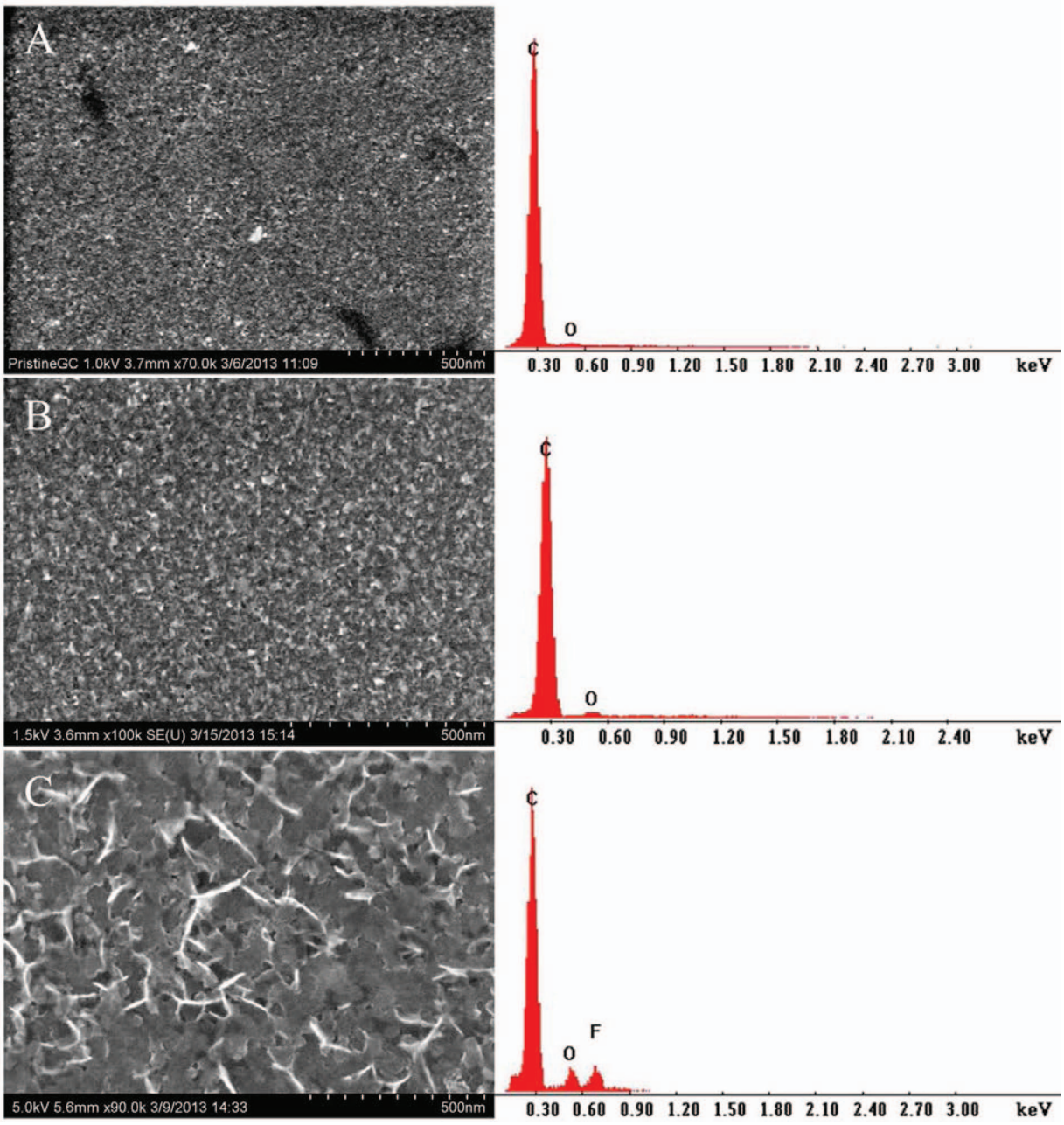

Figure 5. SEM micrographs of the glassy carbon electrode surface, A) pristine electrode, B) after ORR in TBA^+/DMSO, C) after ORR in Li^+/DMSO, d) EDAX analysis of electrode surface after ORR in Li^+/DMSO. Images on the right show the corresponding elemental compositions of the electrode.

glassy carbon disk electrode and supports the view of electrochemical reduction of O_2 followed by chemical decomposition, as displayed in equations 13 and 14.

As an attempt to quantify the passivation of the microelectrode in Li^+ salt solutions after ORR, we have recorded ORR currents on this same microelectrode in $TBAPF_6$ solutions after they have been removed from the ORR in Li^+-containing solutions. Newman et al.[26] have reported that ferrocene oxidation limiting currents can be used as a measure of the amount of passivation at the electrode from solid electrolyte interphase (SEI) formation in lithium ion battery electrolytes. However, our attempts to use ferrocene oxidation as a measure of the extent of passivation due to ORR on the carbon microelectrode, revealed that the bulky ferrocene molecules can overestimate the electrode area passivation. Consequently, we used ORR in the $TBAPF_6$/DMSO solution to determine passivation in Li salt solutions. In this method, involving the reduction of oxygen in a TBA salt solution to measure the extent of electrode passivation from ORR in Li salt solutions, the small oxygen molecules can still penetrate through the pores of any oxide film on the electrode, and give a fair estimate of the extent of passivation from ORR in Li salt solutions. Figure 4D shows the ORR current plateau obtained in a $TBAPF_6$/DMSO solution after an ORR run in 0.1M $LiPF_6$/DMSO. Surprisingly, the extent of passivation is small and insufficient to cause the bell shaped CV response observed in Figure 4B. Therefore, the most probable explanation for the peak-shaped current-voltage response is the migration-diffusion controlled reaction that occurs at the microelectrode[10] as discussed earlier.

The reduction of O_2 to O_2^- in either TBA or Li salt solutions (equation 13) does not involve a charged reactant which can be repelled from the negatively charged electrode. In TBA salt solutions the superoxide is highly stabilized and a second reduction to peroxide does not occur at low overpotentials. On the other hand, the superoxide

reduction to peroxide ions (equation 15) is favored in Li^+ solutions and it starts at a rather low overpotential. However, the negatively charged superoxide ions as soon as they are formed are repelled away from the negatively charged microelectrode surface (in accordance with equation 12 and related discussion earlier) which depletes superoxide concentration below that necessary for the limiting current behavior. In other words, the peak shaped voltammograms in the Li^+ salt solutions appear to arise mainly from mass transport limitations of the superoxide reactant necessary for superoxide reduction to peroxide at the carbon microelectrode. This conclusion is in agreement with the observed large seperation between anodic and cathodic peaks. The superoxide oxidation peaks are not visible on a microelectrode due to (1) efficient removal of the soluble products by the large concentration gradient and (2) due to migration away from the electrode surface by electratstatic repulsion during the negative scan (Figure 4A).

ORR product analysis.— Scanning electron microscopy (SEM) images recorded on the electrode surface after holding the glassy carbon electrode at 2.42 V for 60 min are displayed in Figure 5. The image on the electrode after ORR in TBA^+/DMSO looks similar to the pristine glassy carbon surface whereas the electrode surface after ORR in the presence of Li^+ ions has crystalline product deposits. Energy dispersive spectra (EDAX) were used to characterize this crystalline material detected by SEM images. The oxygen in the passivation product on the microelectrode surface is about 10 atomic percent of the total elements which is consistent with the presence of a lithium oxide layer formed on the electrode surface during the ORR.

Raman spectra obtained for a carbon cloth electrode after potential hold at 2.32 V and 2.12 V are displayed in Figure 6. The lithium oxide products formed were Li_2O_2 at 2.32 V (Figure 6A) and Li_2O at 2.12 V (Figure 6B). The peak at 1088 cm^{-1} in Figure 6A indicates that some Li_2CO_3 is also formed at 2.32 V, produced presumably by the reaction of the Li_2O_2 with atmospheric CO_2 during spectral recording. XRD spectra recorded on Li-O_2 cell cathodes after discharge also showed crystalline Li_2O_2. The formation of Li_2O_2 as the sole product in Li-O_2 cells is due to the potential control of the cell under constant oxygen pressure in the cell.

Irreversibility of oxygen reduction reaction in lithium salt solutions.— The electrochemically irreversible nature of the oxygen reduction reaction in the Li^+ electrolytes in comparison to ORR in TBA^+ electrolytes can be explained by the hard soft acid base (HSAB) concept we previously advanced.[4,7,22] Small cations like Li^+ possessing high charge densities are strong Lewis acids.[22] Superoxide being a soft Lewis base, LiO_2 is unstable and undergoes chemical decomposition/ electrochemical reduction to the more stable Li_2O_2 which is deposited on the electrode surface. At lower potentials, the Li_2O_2 is reduced to Li_2O and appears as the sole product as evidenced by the Raman spectra discussed earlier. This data unequivocally confirms the four-electron reduction of O_2 in DMSO-containing Li salts. The various ORR processes in Li^+ salt solutions are depicted in equations 13–16.

$$Li^+ + O_2 + e^- \rightarrow LiO_2 \quad [13]$$

$$2LiO_2 \rightarrow Li_2O_2 + O_2 \qquad (chemical) \quad [14]$$

$$LiO_2 + Li^+ + e^- \rightarrow Li_2O_2 \quad [15]$$

$$Li_2O_2 + 2Li^+ + 2e^- \rightarrow 2Li_2O \quad [16]$$

The role of the Li salt anion on ORR.—Current voltage characteristics recorded for oxygen purged $LiCF_3SO_3$, $LiClO_4$, $LiN(CF_3SO_2)_2$ electrolytes in DMSO are shown in Figure 7. Similar to the ORR voltammograms observed in $LiPF_6$/DMSO electrolyte, potential dependent (bell shaped) mass transport limited currents were observed in all cases. In contrast to the second reduction reaction ($O_2^- \rightarrow O_2^{2-}$) observed at higher potentials (lower over-potentials) in all electrolytes, there was a significant difference in the magnitude of oxidation peaks observed in different salt solutions. We have calculated the Columbic

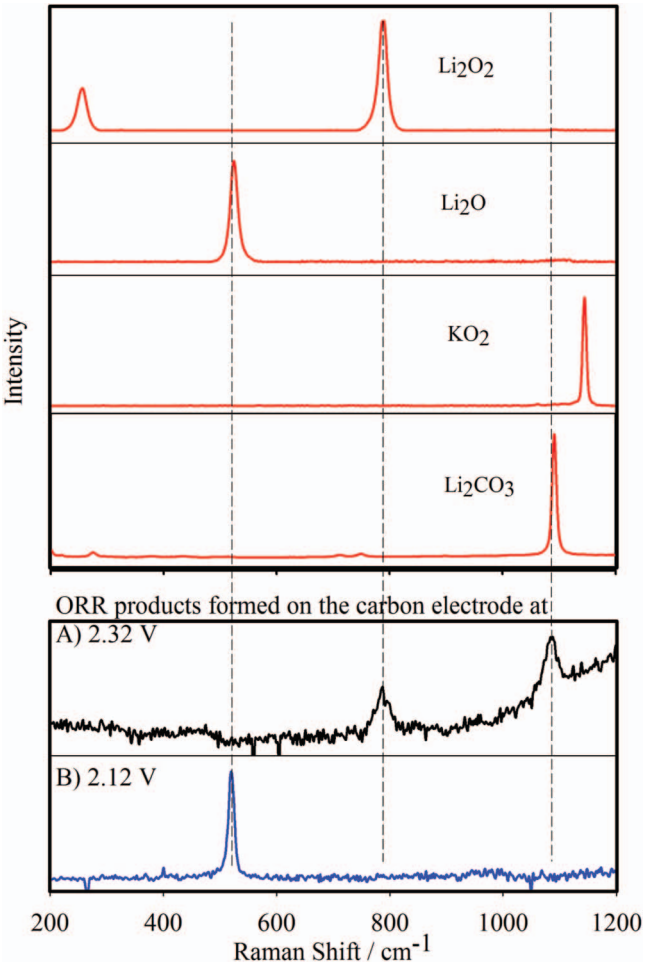

Figure 6. Raman spectra of the oxygen reduction products formed on the carbon electrode; potential hold at A) 2.32 V, B) 2.12 V, each versus Li/Li^+ for 5hrs. Raman spectra for pure reference samples are given in the upper panel.

efficiencies of the OER/ORR reaction (i.e; capacity of OER divided by ORR) in each electrolyte and they are listed as a function of potential sweep rate in Table III. Columbic efficiency is a measure of the amount of insoluble product deposited on the microelectrode since there is minimal contribution from the soluble products accumulated in the double layer as compared to a planer macrodisc electrode.

On a microelectrode, soluble ORR products diffuse away and are not be available for oxidation at the scan rates used here. Then, the oxidation currents observed are for the insoluble products that remain on the electrode surface from the ORR. When the total capacities involved in the ORR processes in the different electrolytes are of the same magnitude, the difference in the columbic efficiencies can be attributed to the differences in the solubility of the reduction products; the higher the solubility of the reduction products, the lower is the columbic efficiency. As shown in Figure 7, the ORR peak currents and the total charge involved in these electrolytes are very similar in the first cycle.

Scan rate dependence of ORR voltammograms in the presence of lithium ions can be explained by the comparison of the rates of superoxide reduction both chemically and electrochemically. At low potential sweeps (1) chemical decomposition of lithium superoxide to lithium peroxide will occur near the electrode, and (2) more peroxides will start to form from the electrochemical reduction of superoxide at higher potentials. Both of these effects lead to instantaneous reduction of the surface activity of the electrode through passivation which in turn leads to low reduction currents. Therefore, an increase in columbic efficiency of ORR by decreasing scan rate is expected

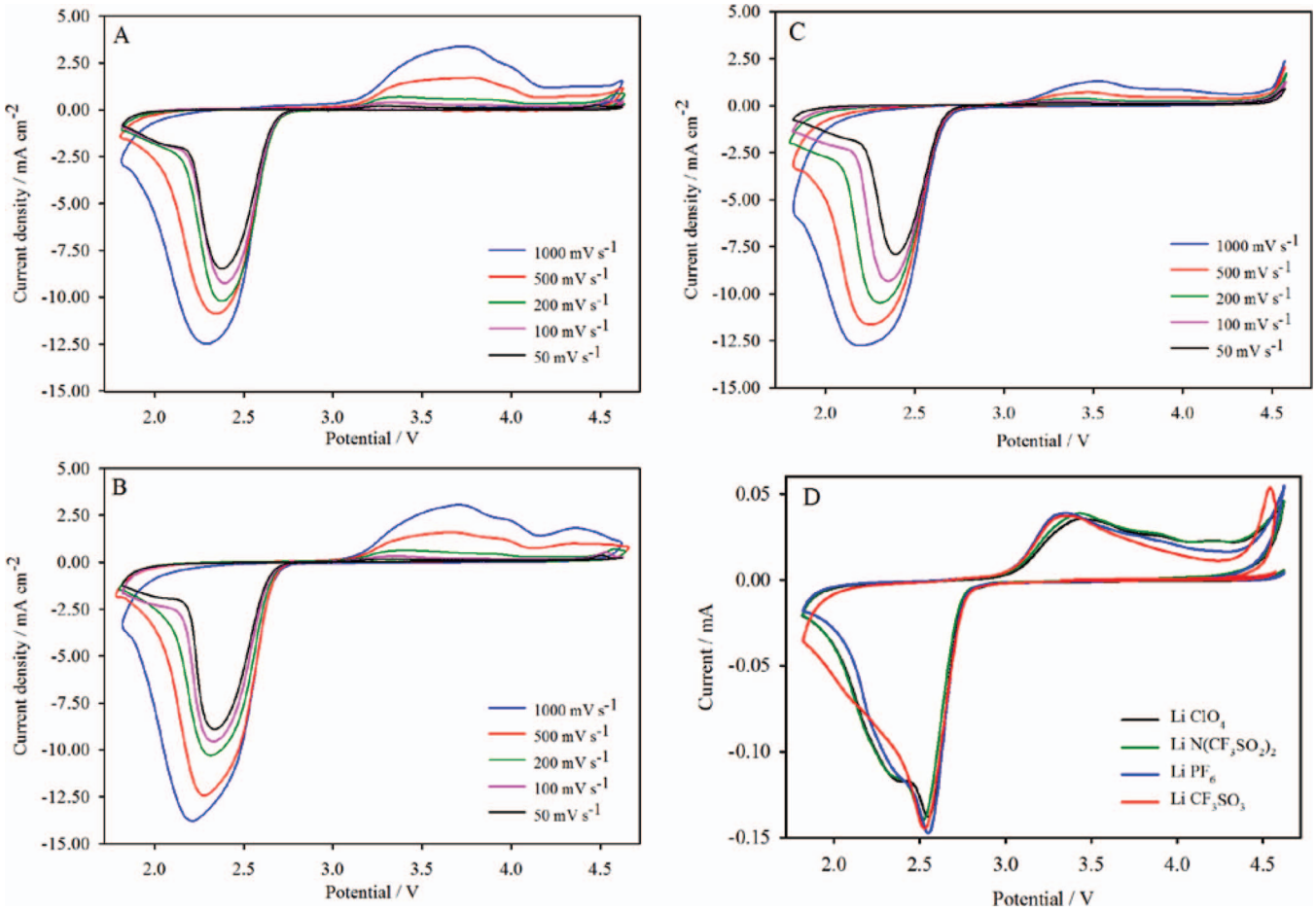

Figure 7. Current-voltage characteristics at the carbon microelectrode obtained for O_2 purged solutions of A) 0.1M $LiClO_4$/DMSO, B) 0.1M $LiN(CF_3SO_2)_2$/DMSO, C) 0.1M $LiCF_3SO_3$/DMSO electrolytes, D) ORR at the Planar GC macroelectrode.

if passivation film formation was the major contributor to columbic efficiency.

Comparison of the Columbic efficiencies (OER/ORR) at scan rates of 200 mVs^{-1} or higher shows that of the four electrolytes, the ORR in the $LiCF_3SO_3$/DMSO has considerably lower columbic efficiency for OER at all scan rates. The observed trend in columbic efficiencies listed in Table III is consistent with product solubility with time since the ORR capacities involved are very similar for all salts. In support of this view, we found that the SEM of the microelectrode surface after the ORR showing much less products in the $LiCF_3SO_3$/DMSO electrolyte than in $LiPF_6$/DMSO. Solubility of Li_2O_2 in a solvent is determined by the solvation energy of its Li^+ cation compared to the lattice energy of this oxide. In the presence of an abundance of DMSO molecules as in a 0.1 M Li salt solution, it is less likely that the Li^+ solvation energies of the electrolytes are significantly different. Therefore, the observed low Li_2O_2 precipitation (higher solubility) in $LiCF_3SO_3$/ DMSO solution is accounted for by the relative strengths of ion pairing, which will be discussed momentarily. Figure 7D shows voltammograms obtained at a planar glassy carbon macrodisc. It is clearly observed that in $LiCF_3SO_3$/DMSO, the second reduction peak appears at a lower potential than that observed in the rest of the electrolytes of interest.

Continuous cycling of the potentials in the cathodic and anodic directions as shown in Figure 8 (carried out in 0.1 M $LiPF_6$/DMSO, and $LiCF_3SO_3$/DMSO electrolytes) showed data consistent with the above conclusion. The anodic limit in these scans was restricted to 3.4 V to allow the ORR lithium oxide products to accumulate on the electrode surface without being oxidized at higher potentials. While similar ORR currents were seen in the first cycle, the ORR current reduction through the 40th scan in $LiCF_3SO_3$/DMSO electrolyte was significantly less and comparable to the reduction current observed in $LiPF_6$/DMSO through just the 10th scan. This suggests that there is less precipitation of the ORR products on the electrode in $LiCF_3SO_3$-containing electrolyte. The higher solubility of the ORR products at least in part may explain the better rechargeability previously observed for Li-air cells utilizing $LiCF_3SO_3$-based electrolytes.[27]

FT-IR evidence for ion pair formation.—FT-IR spectra recorded in $LiPF_6$, $LiCF_3SO_3$, $LiN(CF_3SO_2)_2$ salts in DMSO are shown in

Table III. Columbic efficiencies for OER/ORR (OER divided by ORR) processes in the presence of Li^+ ions.

	Coulombic efficiency at a scan rate of				
Salt	1000 mV s^{-1}	500 mV s^{-1}	200 mV s^{-1}	100 mV s^{-1}	50 mV s^{-1}
$LiPF_6$	46.7%	34.6%	22.3%	17.1%	13.4%
$LiClO_4$	50.1%	34.3%	19.3%	13.2%	7.0%
$LiCF_3SO_3$	16.5%	11.2%	8.2%	6.8%	6.3%
$LiN(CF_3SO_2)_2$	40.0%	26.9%	13.2%	6.5%	3.9%

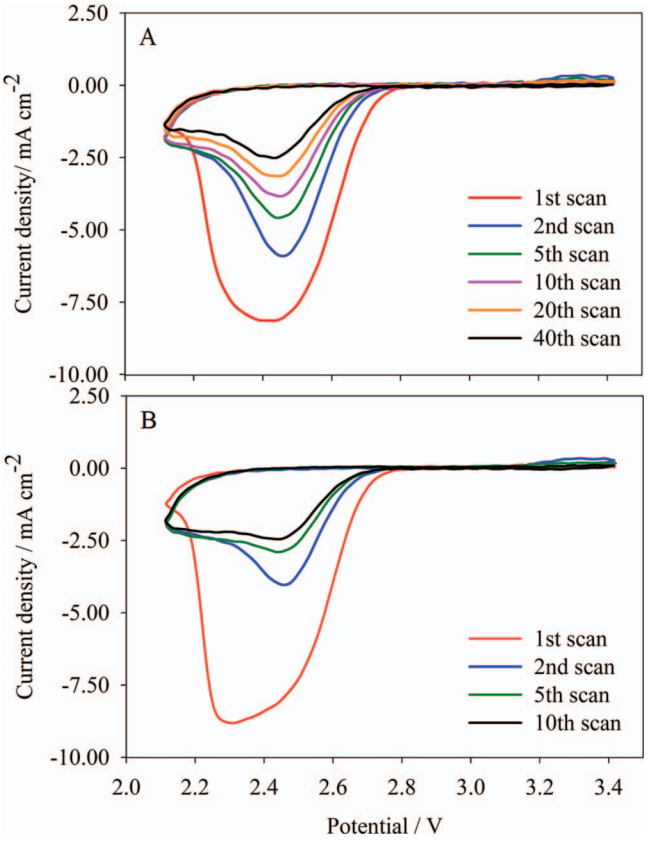

Figure 8. Continuous cycling of potential in O_2 saturated a) $LiCF_3SO_3$/DMSO and b) $LiPF_6$/DMSO electrolytes, at 100 mV s^{-1}.

Figure 9. Spectrum of neat DMSO showed an intense band consisting of two shoulders, at 1050 cm^{-1}. The peak at 1045 cm^{-1} was assigned to the symmetric stretching vibration of the S = O group whereas the shoulder at 1022 cm^{-1} was assigned to rocking vibrations of the methyl groups. Appearance of a new peak at 1028 cm^{-1} with increasing concentration of $LiPF_6$ salt suggests ion pairing between DMSO and lithium ions (Figure 9A). A similar trend was observed in the presence of both $LiN(CF_3SO_2)_2^-$ and $LiCF_3SO_3$ in DMSO. Symmetric stretching vibrations, ν_{ss} of free $CF_3SO_3^-$ ions appear at 1031 cm^{-1}. This new peak leaned toward lower frequencies with the increasing triflate ion concentration, indicating ion pair formation between the S = O of $CF_3SO_3^-$ and Li^+ ions. Asymmetric stretching vibrations (ν_{as}) of free triflate ion appear at 1270 cm^{-1}. When the triflate ions are coordinated with small cations such as Li^+, this peak splits into two peaks, which appears slightly below and above the ν_{as} arising from the free ion. In higher donor number solvents such as DMSO, peaks arising from Li^+ ion paired triflate may not be clearly visible. However, with the increasing concentration of triflate ions, ν_{ss} of free triflate ions shifted toward a lower frequency (Figure 9B inset). It has been reported that the FT-IR peaks arising from Li^+-triflate aggregates appear at 1062 cm^{-1}. We can conclude from these data that as the salt concentration increases the triflate ions form ion pairs and aggregates with the Li^+ in the corresponding electrolyte solution. Surprisingly this lowering of ν_{as} was not observed (Figure 9C) in the ν_{as} peaks from the S = O of $N(CF_3SO_2)_2^-$ ions (ν_{as} = 1352 cm^{-1}). This is explained below in Figure 10, in relation to the ability of contact ion pair formation between Li^+ and the anions in these electrolytes.

Lithium ion-anion ion pair formation.— The trend in the rechargeability of the oxygen half-cell observed above can be explained from the Lewis basicity of the salt anions, which determines the strength of ion pairs formed with the Li^+ cation. First of all, it is important to consider the impact of the solvent molecules themselves on the basicity of the Li^+ ion. Solvation energy for the adduct formation between Li^+ and DMSO can be calculated using the formula in equation 17, developed by Drago et al.[28]

$$-\Delta H = E_A E_B + C_A C_B + R_A T_B \quad [17]$$

In equation 17, ΔH is the enthalpy (in kcal/mole) of formation of a Lewis acid-base adduct, E_A, C_A and R_A are parameters characteristic of the acid (Li^+ here), and E_B, C_B and T_B are parameters characteristic of the base. These parameters for Li^+ are E_A = 11.72, C_A = 1.45 and R_A = 24.21 and these for $(CH_3)_2SO$ are E_B = 2.4, C_B = 1.47, and T_B = 0.65 all values in kcal/mole.[28] The enthalpy of formation calculated for a 1:1 adduct between Li^+ and DMSO is 46.00 kCal/mole whereas that for Li^+ and CH_3CN is 40.34, about 12% lower. A similar trend should follow for adducts of Li^+ formed with a larger number of solvent molecules. Clearly, the higher solvation energy involved in the formation of the complex $Li^+(DMSO)_n$ translates in to lower Lewis acidity for the Li^+ in this solvate than for the Li^+ in $Li^+(CH_3CN)_n$. The higher solvation energy calculated for the solvate formed between DMSO and Li^+ is consistent with that expected from its high donor number of 29.8 compared with a donor number of 14.1 for CH_3CN. These data provide theoretical support for the HSAB concept to explain the ORR mechanism and the products formed in electrolytes prepared with different solvents.

The Li^+ is usually solvated by four solvent molecules to form the solvent-separated ion pairs; e.g., $Li^+(DMSO)_4PF_6^-$, in $LiPF_6$/DMSO electrolyte. Despite its four oxygen atoms, the perchlorate ion (ClO_4^-) cannot form direct ion pair with Li^+ in high donor number solvents like DMSO.[29] Trifluoromethanesulfonate ($CF_3SO_3^-$) (triflate) and bis (trifluoromethanesulfonyl) imide ($N(CF_3SO_2)_2^-$) (trflimide) anions can replace some of the solvent molecules and form direct ion pairs with Li^+ (Figure 10). Most stable coordination is calculated to be bi-dentate for bis(trifluoromethanesulfonyl)imide[30] where the two oxygen atoms come from two different sulfur atoms of the anion. However mono-dentate coordination is the most stable for the trifluoromethanesulfonate anion in polar aprotic solvents.[31] Prior work supports Li^+ coordination with the oxygen atom rather than the nitrogen in the bis(trifluoromethanesulfonyl)imide ion.[30,32] The negative charge on the bis(trifluoromethanesulfonyl)imide ion is delocalized onto neighboring sulfonyl group and as a result it is less available for coordination with the Li^+. Thus, the Lewis basicity of the trifluoromethanesulfonate anion is higher than that of the bis (trifluoromethanesulfonyl) imide anion due to the three electron rich oxygen centers. Consequently, two triflate anions would have a more stable coordination with lithium cations. In fact the donor numbers presented in Table II lend further support for the ability of the triflate ion (with a high donor number of 16.90) to form strong internal coordination with Li^+. The high donor capability of the triflate anion has two possible advantages in the Li-air cathode reaction; it 1) stabilizes the superoxide ions by the softer $Li(triflate)_x^{(n-1)+}(solvent)_y$ cations and mitigates its chemical decomposition/electrochemical conversion to peroxide, 2) possibly helps solvate the Li^+ in Li_2O_2 leading to some solubility for the peroxide in the $LiCF_3SO_3$/DMSO electrolyte and removing it from the electrode surface to mitigate electrode passivation. Our experimentally observed trend in Columbic efficiencies suggests possible contributions from both of these effects. Note that on the microelectrode, soluble products would diffuse away quickly from the electrode surface making it unavailable for oxidation, while insoluble products that remain on the electrode surface are more efficiently oxidized. The results presented here indicate a unique role for the triflate anion on ORR in DMSO and point out the ability of microelectrode data to help diagnose the role of the Li salt on O_2 electrode reversibility in the Li-air cell.

Oxygen reduction kinetics in TBA and Li salt- based electrolytes.— We have plotted $E - E^0$ vs. $[(i_l - i)/i] - [(i_l - i^r)/i^r]$ (as shown in equation 10) for the four Li^+-based electrolyte systems (Figure 11). Currents observed in the corresponding TBA electrolyte have been used as the current values in reversible system. The transfer

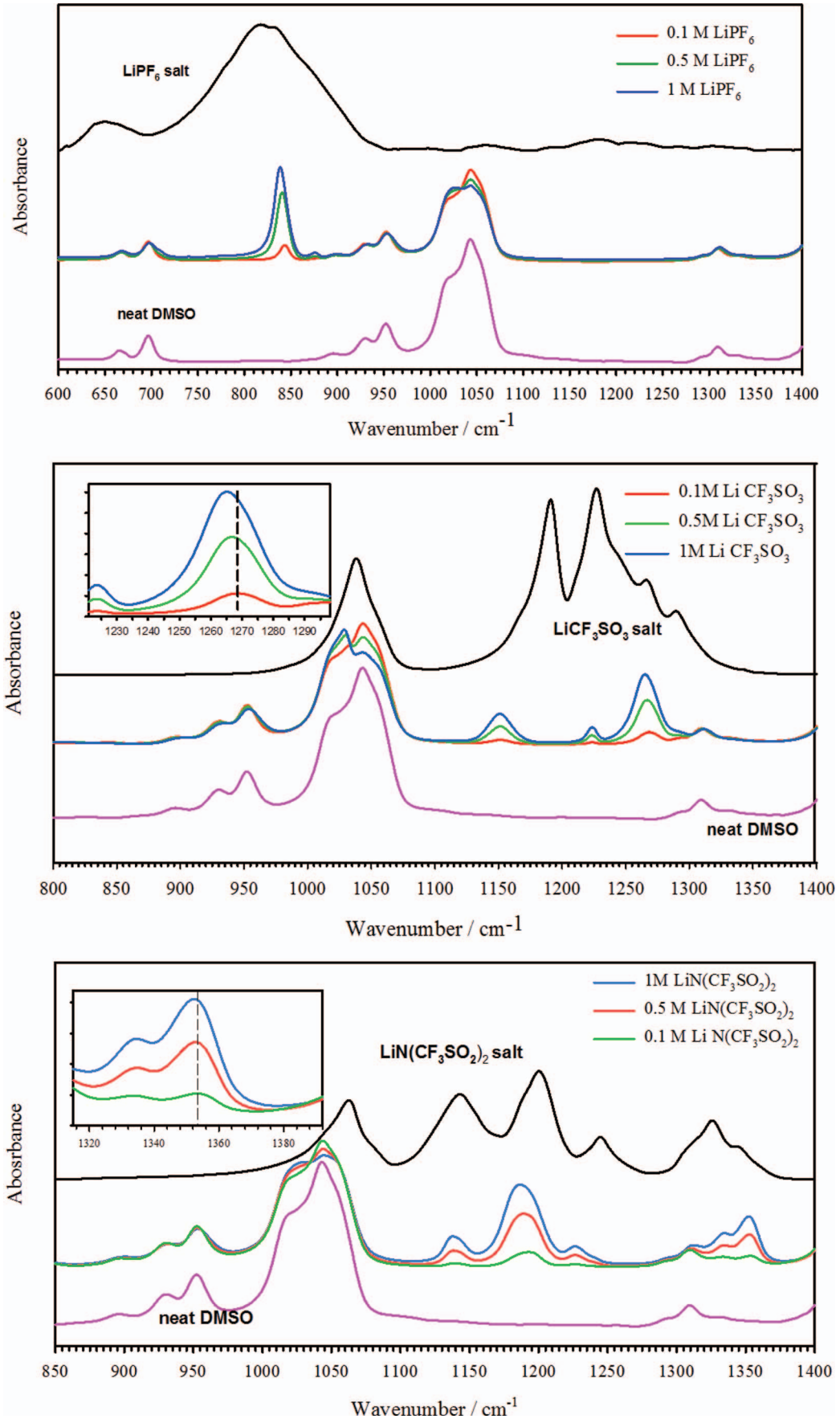

Figure 9. FT- IR spectra of TEGDME-Lithium salt solutions. (A) $LiPF_6$-DMSO, (B) Li CF_3SO_3-DMSO, (C) $LiN(CF_3SO_2)_2$ –DMSO.

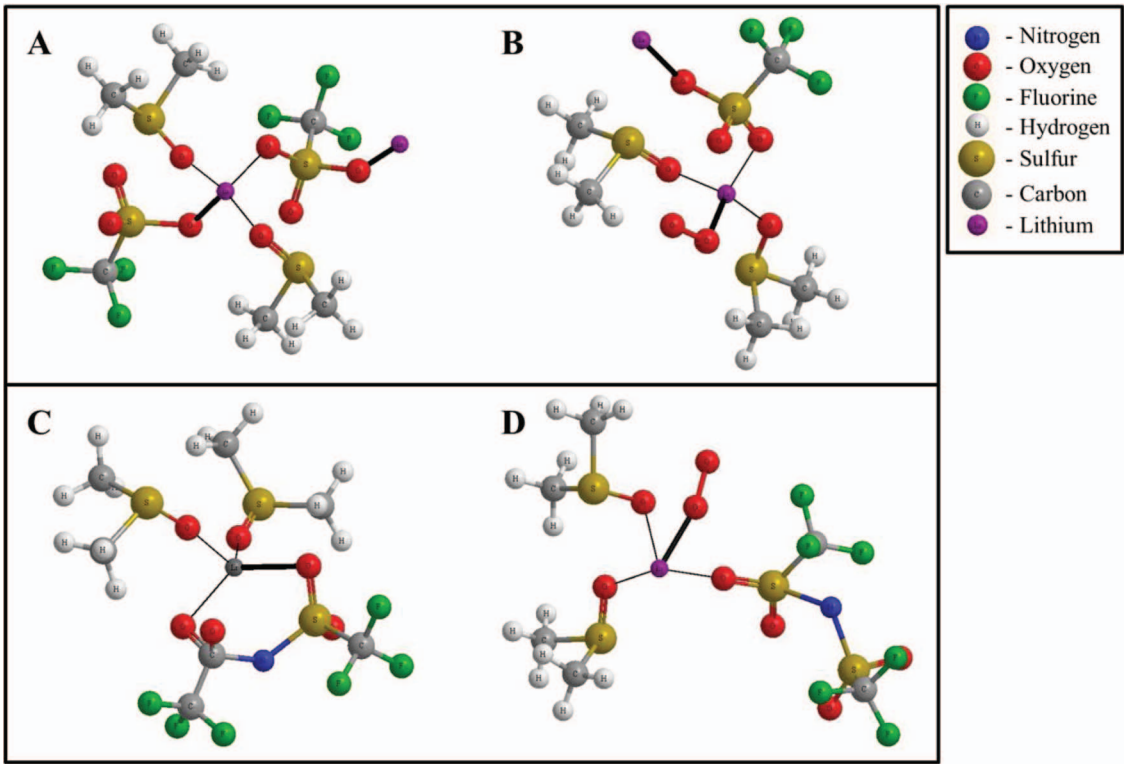

Figure 10. Solvation and contact ion pair formation in A) $LiCF_3SO_3$/DMSO and C) $LiN(CF_3SO_2)_2$/DMSO electrolytes. Ion pair between solvated Li^+ and superoxide ion in B) $LiCF_3SO_3$/DMSO, D) $LiN(CF_3SO_2)_2$/DMSO electrolytes.

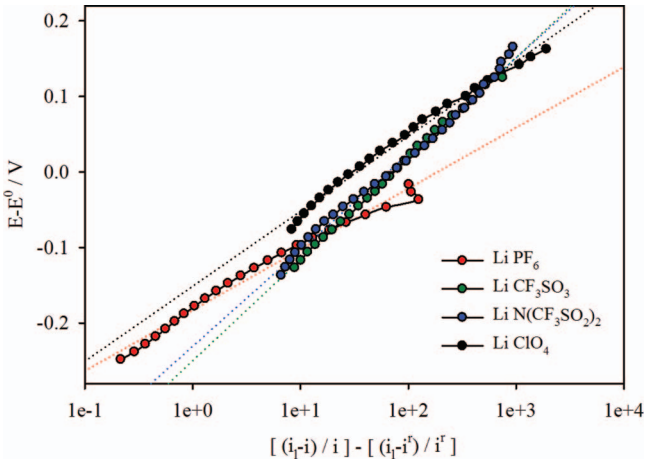

Figure 11. Calculation of kinetic parameters for the quasi-reversible ORR in Li^+-containing electrolytes with various anions.

coefficient, α, and the heterogeneous rate constant, k_s, calculated are shown in Table IV. According to the data in Tables I and II, the size of the cation does not have a significant impact on the viscosity or oxygen transport parameters in DMSO. Therefore, in the presence of Li^+ ions, it is reasonable to use the limiting current in TBA^+/DMSO electrolyte for that in Li^+/DMSO electrolytes. Apart from the large differences between TBA^+ and Li^+ salts, comparison of the voltammetric responses obtained in different Li^+-based electrolytes revealed valuable distinguishing features. In $LiCF_3SO_3$/DMSO and $Li(CF_3SO_2)_2N$/DMSO solutions, transfer coefficients are close to 0.5 whereas in $LiPF_6$/DMSO a much low transfer coefficient (~0.3) was observed. The slow kinetics observed in $LiPF_6$/DMSO can be possibly attributed to the electrode surface modified with insoluble products formed at high potentials. A transfer coefficient of 0.57 in the triflate electrolyte suggests a more desirable ORR and OER kinetics in this electrolyte.

Table IV. Kinetic parameters of ORR in Li^+-based electrolytes.

Salt	Transfer coefficient: α
$LiPF_6$	0.28
$LiClO_4$	0.42
$LiCF_3SO_3$	0.57
$LiN(CF_3SO_2)_2$	0.54

Conclusions

We have found that microelectrode can be used as a diagnostic tool to select and optimize the properties of electrolytes for non-aqueous Li-air batteries, and to elucidate O_2 redox reaction mechanisms in presence of different ion-conducting salts. Distinct differences were observed in the current-voltage response of a microelectrode in oxygen saturated DMSO solutions containing a series of TBA^+ and Li^+ salts. The characteristic limiting currents observed in TBA^+ salt solutions due to the exceptional stability and solubility of the ORR products were contrasted with the bell shaped CV responses in Li^+ salt solutions, attributed to the passivation of the microelectrode surface by insoluble ORR products combined with the electrostatic repulsion of O_2^-, the initial O_2 reduction product. The final O_2 reduction products were identified be Li_2O_2 and Li_2O formed at different potentials. Our data confirm the four-electron reduction of O_2 to Li_2O in DMSO. Overall oxygen transport was not influenced by anion of either the TBA or Li salts. The trend in OER/ORR coulombic efficienies in Li^+-based electrolytes suggested that there is improved O_2^- stability and ORR product solubility in $LiCF_3SO_3$/DMSO electrolytes, probabaly due to increased solvation of the Li^+ cation by the triflate anion which

may translate into better ORR and OER kinetics for the Li-air cell utilizing this electrolyte as previously observed.[27]

Acknowledgment

We sincerely thank U.S. Army CERDEC for the finacial support provided through subcontract No. GTS-S-13-025 for this work.

References

1. K. M. Abraham, P. G. Bruce, and L. J. Hardwick, *MRS Bull*, **36**, 506 (2011).
2. J. Christensen, P. Albertus, R. S. Sanchez-Carrera, T. Lohmann, B. Kozinsky, R. Liedtke, J. Ahmed, and A. Kojic, *Journal of The Electrochemical Society*, **159**, R1 (2011).
3. K. M. Abraham and Z. Jiang, *Journal of The Electrochemical Society*, **143**, 1 (1996).
4. C. O. Laoire, S. Mukerjee, K. M. Abraham, E. J. Plichta, and M. A. Hendrickson, *The Journal of Physical Chemistry C*, **114**, 9178 (2010).
5. B. D. McCloskey, D. S. Bethune, R. M. Shelby, G. Girishkumar, and A. C. Luntz, *The Journal of Physical Chemistry Letters*, **2**, 1161 (2011).
6. M. J. Trahan, S. Mukerjee, E. J. Plichta, M. A. Hendrickson, and K. M. Abraham, *Journal of The Electrochemical Society*, **160**, A259 (2013).
7. C. O. Laoire, S. Mukerjee, K. M. Abraham, E. J. Plichta, and M. A. Hendrickson, *The Journal of Physical Chemistry C*, **113**, 20127 (2009).
8. Y. Wang, D. Zheng, X.-Q. Yang, and D. Qu, *Energy & Environmental Science*, **4**, 3697 (2011).
9. D. Zheng, X. Q. Yang, and D. Qu, *Chemistry–An Asian Journal*, **6**, 3306 (2011).
10. J. D. Norton, H. S. White, and S. W. Feldberg, *Journal of Physical Chemistry*, **94**, 6772 (1990).
11. M. I. Montenegro, M. A. Queirós, and J. L. Daschbach, *Microelectrodes: Theory and Applications*, Springer (1991).
12. W. Xu, J. Xiao, D. Wang, J. Zhang, and J.-G. Zhang, *Journal of The Electrochemical Society*, **157**, A219 (2010).
13. W. Xu, J. Xiao, J. Zhang, D. Wang, and J.-G. Zhang, *Journal of The Electrochemical Society*, **156**, A773 (2009).
14. C. J. Allen, S. Mukerjee, E. J. Plichta, M. A. Hendrickson, and K. M. Abraham, *The Journal of Physical Chemistry Letters*, **2**, 2420 (2011).
15. A. J. Wain, G. G. Wildgoose, C. G. R. Heald, L. Jiang, T. G. J. Jones, and R. G. Compton, *The Journal of Physical Chemistry B*, **109**, 3971 (2005).
16. P. Shi, I. Fromondi, and D. A. Scherson, *Langmuir*, **22**, 10389 (2006).
17. J. Janisch, A. Ruff, B. Speiser, C. Wolff, J. Zigelli, S. Benthin, V. Feldmann, and H. A. Mayer, *Journal of Solid State Electrochemistry*, **15**, 2083 (2011).
18. K. Aoki and J. Osteryoung, *Journal of Electroanalytical Chemistry and Interfacial Electrochemistry*, **122**, 19 (1981).
19. C. P. Winlove, K. H. Parker, and R. K. C. Oxenham, *Journal of Electroanalytical Chemistry and Interfacial Electrochemistry*, **170**, 293 (1984).
20. A. J. Bard and L. R. Faulkner, *Electrochemical methods: fundamentals and applications*, Wiley New York (1980).
21. Z. Galus, J. Golas, and J. Osteryoung, *The Journal of Physical Chemistry*, **92**, 1103 (1988).
22. C. J. Allen, J. Hwang, R. Kautz, S. Mukerjee, E. J. Plichta, M. A. Hendrickson, and K. M. Abraham, *The Journal of Physical Chemistry C*, **116**, 20755 (2012).
23. D. T. Sawyer and J. L. Roberts, Jr, *Journal of Electroanalytical Chemistry (1959)*, **12**, 90 (1966).
24. D. T. Sawyer, G. Chiericato, C. T. Angelis, E. J. Nanni, and T. Tsuchiya, *Analytical Chemistry*, **54**, 1720 (1982).
25. W. Linert, A. Camard, M. Armand, and C. Michot, *Coordination Chemistry Reviews*, **226**, 137 (2002).
26. M. Tang and J. Newman, *Journal of The Electrochemical Society*, **158**, A530 (2011).
27. H.-G. Jung, J. Hassoun, J.-B. Park, Y.-K. Sun, and B. Scrosati, *Nature Chemistry*, **4**, 579 (2012).
28. R. S. Drago, D. C. Ferris, and N. Wong, *Journal of the American Chemical Society*, **112**, 8953 (1990).
29. Y. M. Cahen, P. R. Handy, E. T. Roach, and A. I. Popov, *The Journal of Physical Chemistry*, **79**, 80 (1975).
30. R. Arnaud, D. Benrabah, and J. Y. Sanchez, *The Journal of Physical Chemistry*, **100**, 10882 (1996).
31. W. Huang, R. Frech, and R. A. Wheeler, *The Journal of Physical Chemistry*, **98**, 100 (1994).
32. J. L. Nowinski, P. Lightfoot, and P. G. Bruce, *Journal of Materials Chemistry*, **4**, 1579 (1994).